EUROfusion

EUROFUSION CP(15)07/04

M.J. Mantsinen et al.

Analysis of ICRF Heating and ICRF–Driven Fast Ions in Recent JET Experiments

14th IAEA Technical Meeting on Energetic Particles in Magnetic Confinement Systems
Vienna, Austria
(1st September 2015 – 4th September 2015)

This work has been carried out within the framework of the EUROfusion Consortium and has received funding from the Euratom research and training programme 2014-2018 under grant agreement No 633053. The views and opinions expressed herein do not necessarily reflect those of the European Commission.

Analysis of ICRF heating and ICRF-driven fast ions in recent JET experiments

M.J. Mantsinen[1,2,a], C. Challis[3], J. Eriksson[4], L.-G. Eriksson[5], D. Frigione[6], D. Gallart[2], J. Garcia[7], C. Giroud[3], T. Hellsten[8], A. Hjalmarsson[4], D.B. King[3], V. Kiptily[3], E. Lerche[9], M. Santala[10], M. Schneider[7], S. Sharapov[3] , D. Van Eester[9] and JET contributors*

EUROfusion Consortium, JET, Culham Science Centre, Abingdon, OX14 3DB, UK
[1]ICREA, Barcelona, Spain
[2]Barcelona Supercomputing Center, Barcelona, Spain
[3]CCFE, Culham Science Centre, Abingdon, OX14 3DB, UK
[4]Uppsala University, Department of Physics and Astronomy, Sweden
[5]European Commision, Brussels, Belgium
[6]ENEA, Frascati, Italy
[7]CEA, IRFM, 13108 Saint-Paul-lez-Durance, France
[8]Dept. of Fusion Plasma Physics, EES, KTH, Stockholm, Sweden
[9]Laboratory for Plasma Physics, LPP-ERM/KMS, Brussels, Belgium
[10]Aalto University, Espoo, Finland.
**See Appendix of F. Romanelli et al., Proc. 25th IAEA FEC 2014, Saint Petersburg, Russia*
[a]email address of the corresponding author: mervi.mantsinen@bsc.es

Abstract

Heating with waves in the ion cyclotron range of frequencies (ICRF) is a well-established method on present-day tokamaks. ICRF waves will also be used in ITER and are planned for the demonstration fusion power plant DEMO. The present paper analyses ICRF heating in recent experiments on the JET tokamak with the ICRF modelling code PION. Special emphasis is given on second and higher harmonic heating schemes ($\omega \approx n\omega_{ci}$, $n \geq 2$) in preparation of ITER. The results show that the theoretical picture of heating at the harmonics of the ion cyclotron frequency on which PION is based is reasonably correct. This gives confidence in the simulations of other experiments on JET and in the extrapolations of ICRF heating to ITER and future reactor plasmas.

1. Introduction

Heating with waves in the ion cyclotron range of frequencies (ICRF) plays an important role in the operation and the performance optimization of several present-day experimental fusion devices. ICRF waves will also be used in ITER and are planned for the demonstration fusion power plant DEMO. For ITER, the main ICRF scenario is the second harmonic heating of tritium ($\omega \approx 2\omega_{cT}$) which coincides with the fundamental minority heating of ^{3}He. For second harmonic heating of tritium, as for other harmonic ICRF heating schemes, the damping of the wave power is a finite Larmor radius effect. Its physics can be studied in the present day experiments using ICRF schemes involving second or high harmonic damping ($\omega \approx n\omega_{ci}$, $n \geq 2$). Recently, important aspects of the scheme have been explored on the JET tokamak with the ITER-like wall [1] in plasmas with ICRF heating alone and with combined neutral beam injection (NBI) and ICRF heating. Since for higher-harmonic heating the absorption strength,

and thus the ICRF power partition among different absorbing species, depend strongly on the distribution function, such scenarios are particularly challenging to model. In the present paper, recent experiments in JET are analysed with the ICRF modelling code PION [2] with special emphasis on the physics of higher harmonic heating. We consider three series of experiments with different ICRF scenarios for which second or higher harmonic damping plays an important role: (a) hydrogen minority heating, coinciding with second harmonic heating of deuterium beam ions, in high-performance discharges; (b) third harmonic heating of deuterium beam ions for fusion product studies [3] and (c) second harmonic heating of hydrogen in hydrogen plasmas [4]. Comparisons between the experimental results with modelling are presented, with special emphasis on the comparisons of the simulated ICRF-induced enhancement of the neutron rate and ICRF-accelerated fast deuterium distribution functions with those measured with the neutron time-of-flight spectrometer TOFOR [5].

2. ICRF modelling with the PION code

In the present paper the ICRF modelling code PION [2] is used to analyse ICRF heating and ICRF-driven fast ions at JET. PION provides a self-consistent and time-dependent calculation of the ICRF power deposition and the pitch-angle averaged velocity distribution(s) of the resonating ions. It is based on simplified models and, therefore, it is relatively fast, which makes an analysis of a large number of discharges feasible. Furthermore, PION takes into account the synergy with NBI [6], which is particularly important for the analysis of the present discharges. Finite-orbit-width effects are taken into account by noting that the fast ions have turning points close to the cyclotron resonance and by averaging the collision coefficients over those orbits.

In the course of the analysis reported in this paper, the PION code has been further developed. This work has been motivated by detailed comparisons with the measured ICRF-driven fast ion distribution functions up into the multi-MeV energy range. They have confirmed that in the experimental conditions where the ICRF power is large enough to drive a significant ICRF-driven fast ion tail, the resulting fast ion distribution function can decrease sharply due to finite Larmor radius effects around the first local minimum of the ICRF diffusion coefficient $D_{RF}(v,\mu) \propto \sum_N \left|E_+ J_{n-1}(k_\perp \rho) + E_- J_{n+1}(k_\perp \rho)\right|^2 \approx 0$. Here, v is the velocity, μ is the cosine of the pitch-angle of the ion relative to the background magnetic field, the sum goes over the toroidal mode number *N* spectrum of the launched wave, $k_\perp$ is the component of the wave vector perpendicular to the background magnetic field, $\rho = v\sqrt{1-\mu^2}\,/\,\omega_{ci}$ is the Larmor radius, J_n is the Bessel function of first kind, and E_+ and E_- are the left-hand and right-hand components of the wave electric field, respectively. This happens when wave-particle interaction is suppressed due to finite Larmor radius effects and acts as a barrier for phase space diffusion to higher energies [7, 8]. In order to include this effect in the modelling of the pitch-angle-averaged distribution function as in PION, it was found that the pitch-angle-averaging of the ICRF diffusion coefficient plays a key role. Previous to this work, the pitch-angle-average of $D_{RF}(v,\mu)$ in PION was calculated as $\frac{1}{2}\int_{-1}^{1} D_{RF}(v,\mu)d\mu$ [2] which was found to give good results apart from the proximity of the barrier, where it is not able reproduce the sharp decrease of the distribution function as observed in the experiments. This was found to be due to the spread in the location of the minimum of $D_{RF}(v,\mu)$ for different μ which effectively smears out the barrier. Such spreading is not physical because the ICRF waves tend to drive an anisotropic fast ion population of predominantly trapped resonant ions with $\mu \approx 0$ which absorb significant fraction of the available power. Improved agreement between

the measured and simulated distribution functions around the barrier is obtained with a new pitch-angle-averaged ICRF diffusion coefficient based on a simple model for the pitch-angle-dependent distribution function $f(v,\mu)$ which is used as a weight function in the pitch-angle-averaging of $D_{RF}(v,\mu)$ as detailed in Appendix. In this paper, first PION results with the upgraded $D_{RF}(v,\mu)$ are presented. In our future work, we plan to assess this model further against experimental pitch-angle-resolved fast ion data and/or other ICRF modelling codes.

3. ICRF heating of high-performance hybrid discharges

Finite Larmor radius effects play an important role in JET high-performance discharges with combined NBI and ICRF heating. Here, we analyse three discharges 86614, 87331 and 86871 from the JET hybrid scenario development aimed at designing a plasma regime capable of long pulse operation with a combination of inductive and non-inductive current drive. The overview of the main discharge parameters are shown in Fig. 1. Discharges 86614 and 86871 were carried out at a toroidal magnetic field B_T of 2.9 T and a plasma current I_p of 2.5 MA, while B_T of 1.95 T and I_p of 2.1 MA was used for discharge 87331. Up to 22 MW of D NBI was applied with injection energies in the range of 90-115 keV. In discharges 86614 and 86871 up to 5 MW of ICRH power was applied at a frequency of 42.5 MHz while in discharge 87331 up to 2.5 MW of ICRH power was used at 32.4 MHz. In all discharges the $0\pi0\pi$ phasing of the ICRF antennas was used (i.e. $k_{||} \approx 9\ m^{-1}$ at the peak of the ICRF power spectrum). The $\omega \approx \omega_{cH} = 2\omega_{cD}$ resonance was located at R_{res}–R_0 of 2.5 cm, -33 cm and 9 cm at the peak performance for discharges 86614, 87331 and 86871, respectively. Here, R_{res} and R_0 are the major radii of the resonance and magnetic axis, respectively. The best performing discharge 86614 reached a normalized beta β_N of 2.1 and a confinement factor H98 of 1.1. The duration of the high-power phase was limited by impurity accumulation.

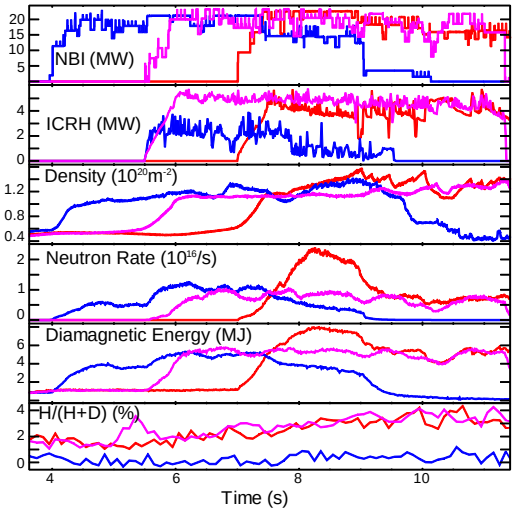

Figure 1 NBI and ICRH power, line-integrated electron density, neutron yield, plasma diamagnetic energy and hydrogen concentration for JET hybrid discharge 86614 (red), 87331 (blue) and 86871 (magenta).

For the $\omega \approx \omega_{cH} = 2\omega_{cD}$ scenario, the ICRF power partitioning between the resonant hydrogen minority and deuterium ions depends on the hydrogen concentration $n_H/(n_H+n_D)$ and the deuterium energy density [6]. The hydrogen concentration, deduced from the ratio of the D_α and H_α light collected along lines of sight through the plasma, was 2-3% in discharges 86614 and 86871 and below 0.5% in discharge 87331. Penning gauge spectroscopy in the divertor gave somewhat higher $n_H/(n_H+n_D)$ values of 2-4%, 3-5% and 1-2% for discharges 86614, 86871 and 87331, respectively.

In discharges 86614 and 86871, up to ≈20%, 70-75% and 5-10% of the ICRF power is absorbed, respectively, by D ions at $\omega \approx 2\omega_{cD}$, hydrogen minority ions at $\omega \approx \omega_{cH}$ and by direct electron damping by electron Landau damping and transit time magnetic pumping. In discharge 87331 damping by hydrogen minority ions is reduced due to a lower $n_H/(n_H+n_D)$. The best agreement with the measured data is obtained assuming a very low $n_H/(n_H+n_D)$ of < 0.1%. As result, the H damping is negligible, while direct electron damping and D damping take 45% and 55% of the ICRF power, respectively. The ICRF power transferred collisionally from the fast ions to the bulk ions is about 2, 2.5 and 1 MW for discharges 86614, 86871 and 87331, respectively, the rest being transferred to the plasma electrons. The ICRF power is deposited centrally inside r/a < 0.5, where r/a is the normalised plasma minor radius.

The comparisons of the simulated and measured plasma diamagnetic energy content W_{DIA} and total neutron rate R_{NT} are shown in Fig. 2 for discharge 86871. The agreement between modelling and experimental results is remarkably good. Similar agreement is found for discharges 86614 and 87331. The thermal contribution to W_{DIA} is about 75% while the non-thermal component is about 25%.

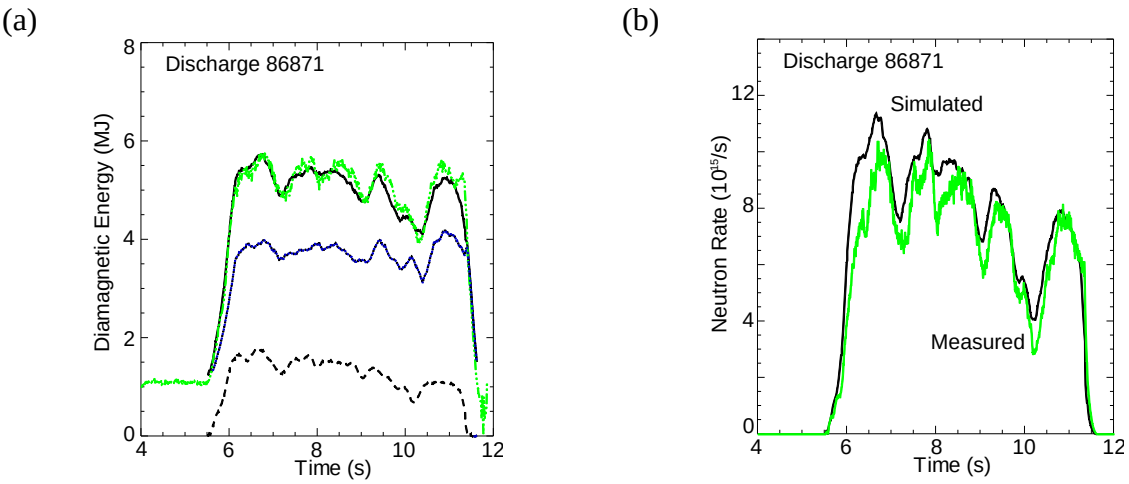

Figure 2 (a) Measured (green) and simulated (solid black) total plasma diamagnetic energy content together with the measured thermal (dotted blue) and simulated nonthermal (black dashed) contributions for discharge 86871. (b) Measured (green) and simulated (black) total neutron rate for discharge 86871.

According to PION, up to 5-20% of R_{NT} is due to the second-harmonic D acceleration. The predicted ICRF enhancement of R_{NT} has been compared [9] with the results of the time-of-flight neutron spectrometer TOFOR [5] and good agreement has been found. Figure 3 shows the comparison for discharge 87731. In spite of having the lowest coupled ICRF power, this discharge shows the largest ICRF enhancement of R_{NT} due to the lowest $n_H/(n_H+n_D)$ which is favourable for deuterium damping.

4. Third harmonic heating of deuterium beam ions for fusion product studies

We have modelled ICRF heating and ICRF-accelerated fast deuterium tails in recent JET experiments aimed at studying fusion products [3]. These experiments used a combination of deuterium NBI and ICRF heating tuned to the central $\omega \approx 3\omega_{cD}$ resonance to drive fast deuteron NBI ions to high energies. Here, we concentrate our analysis on discharges where no ^{3}He was introduced in the plasma. Discharges with ^{3}He have been modelled using the SELFO-light code and are reported elsewhere [10].

In our earlier work [11], the $\omega \approx 3\omega_{cD}$ scheme without deuterium NBI on JET was modelled with the PION code. To obtain a consistent picture with the experimental data, fast ion orbit losses and parasitic damping at the plasma edge needed to be accounted for. Furthermore, sawtooth redistribution of fast ions was found to be important at higher sawtooth frequencies. In the analysis of the recent experiments, we use the same physics model apart from sawtooth redistribution which we have not considered so far. As in [11], parasitic damping is introduced by adding a fictitious species with a cyclotron resonance at the plasma edge. In the simulations presented here, single pass damping of 30% is used for the fictitious species.

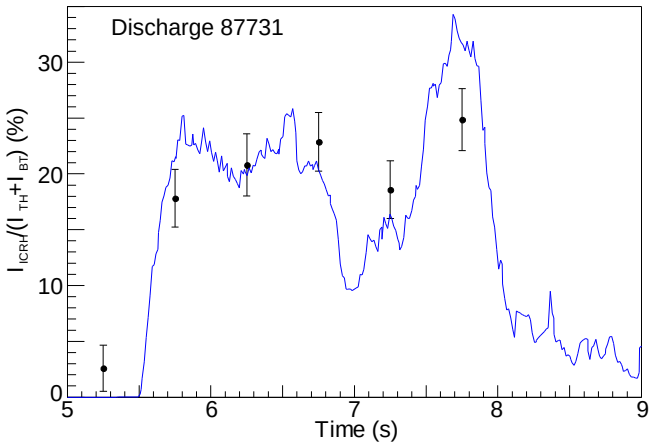

Figure 3 Enhancement of the neutron rate due to second harmonic D damping according to PION (blue) and TOFOR (points with error bars, integrated over 0.5 s) for discharge 87731.

We consider first discharges 86464 and 86459 which were prepared in a different way to vary the ICRF-driven fast deuteron tail at B_T of 2.25 T and I_p of 2.15 MA. In discharge 86459 up to 4.5 MW of D NBI was applied with injection energies in the range of 80-120 keV, while in discharge 86464 up to 2.6 MW of D NBI was used with injection energies of 80-100 keV. In addition, up to 2.9 MW and 4.0 MW of ICRF power was applied in discharges 86459 and 86464, respectively, with an ICRF frequency of 51.5 MHz using the $0\pi0\pi$ phasing of the ICRF antennas. The $\omega \approx 3\omega_{cD}$ resonance was located at $R_{res}–R_0 \approx$ 10-15 cm while the central electron density was increased from $4.2\text{x}10^{19}$ m^{-3} in discharge 86459 to $5\text{x}10^{19}$ m^{-3} in discharge 86464 to change the wave characteristics.

As a result of the above differences, the plasma performance is significantly different in the two discharges. In particular, in discharge 86459 R_{NT} of $6\text{x}10^{15}$ s^{-1} and W_{DIA} of 2.5 MJ are obtained which are a factor of 2.3 and 1.4 higher, respectively, than those obtained in discharge 86464. Significant differences are also observed in the measured deuterium distribution functions as deduced from TOFOR [5] measurements along a vertical line of sight through the plasma center (Fig. 4). These differences are consistent with an expected difference in the location of the local minimum of D_{RF} due to finite Larmor radius effects as the wave characteristics are modified by the change in the plasma density. This is confirmed by the deuterium distributions functions as simulated by PION for the two discharges and also shown in Fig. 4. Good overall agreement is obtained for both discharges in discharge 86459 apart from the low energy range below 0.4 MeV, the reasons of which are being investigated. According to PION, the deuterium damping is about 60-65% and the parasitic edge damping 20-30% and direct electron damping 10-15% of the total power. Comparisons with other fast ion measurements and ICRF modelling codes are given in Ref. [12,13].

One of our next aims is to compare the time behaviour of the measured and simulated distribution functions in discharge 86768 in order to study the dynamics of the ICRF-driven

fast ion tail. This discharge is well suited for the purpose because it had a notch in the NBI power from 3 MW to 1.4 MW from t = 11 s to t = 12 s and a fast ICRF power switch-off at 13 s towards the end of the discharge. Up to 4 MW of ICRF power was applied at a frequency of 51.4 MHz using the $0\pi0\pi$ phasing at B_T of 2.2T and I_p of 1.95 MA. The $\omega \approx 3\omega_{cD}$ resonance was located at R_{res}–R_0 of 7-10 cm. According to PION, stepping down the NBI power decreases deuterium single pass damping from about 80% to about 40%, which gives rise to a concomitant increase in the fraction of ICRF power damped parasitically at the plasma edge (c.f. Fig. 5) and a significant decrease in the ICRF-drivan fast deuteron tail (c.f Fig. 6). In terms of the global parameters R_{NT} and W_{DIA} and their time evolution, PION is in good agreement with the measured data as shown in Fig. 7.

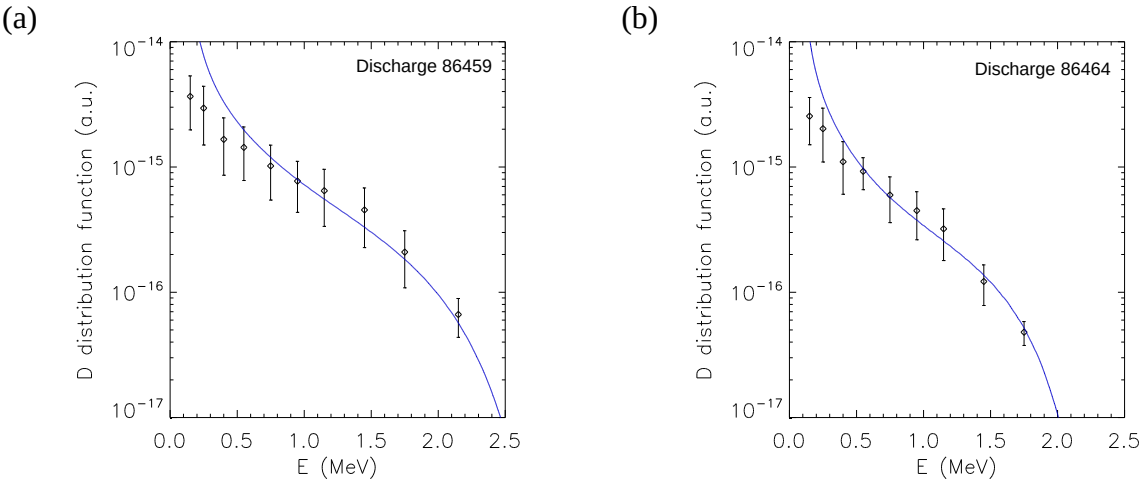

Figure 4 Deuterium distribution function f(v, μ= 0) as given by PION at t = 12.5 s and the deuterium distribution function as deduced from the TOFOR [5] measurements (diamonds; integrated in time from t = 11.5 to 12.5 s) for (a) discharge 86459 and (b) discharge 86464 with third harmonic heating of deuterium beam ions on JET.

5. Second harmonic heating of hydrogen in hydrogen plasmas

In recent experiments on JET good ICRF heating efficiency and transition into H-mode confinement have been demonstrated with ICRF heating alone using $\omega \approx 2\omega_{cH}$ in hydrogen plasmas with $n_H/(n_H+n_D)$ of 99% [4]. These experiments were carried out at B_T of 1.8 T and I_p of 1.45-1.65 MA. Up to 6.2 MW of ICRH power was applied at a frequency of 51.4 MHz using the $0\pi0\pi$ phasing. The $\omega \approx 2\omega_{cH}$ resonance was located off-axis at R_{res}–R_0 of 25-35 cm. Here, we will concentrate our analysis on discharges 87869-87877 with central electron densities above $2.5\text{x}10^{19}/\text{m}^3$ and central electron temperatures in the range of 0.9-2.1 keV

In these experimental conditions, according to PION, hydrogen absorbs about 95% of the total ICRF power, and the rest goes to direct electron damping. As a result, a fast ion tail forms in the distribution function of the hydrogen ions. However, given the low average power per particle for the off-axis resonance together with the efficient slowing down of fast ions at the relatively low plasma temperatures, the calculated fast ion tails are rather modest. As shown in Fig. 8a, the simulated fast ion energy content increases in these conditions more rapidly than the scaling $W_{fast} = P_{ICRF}\tau_{SD}/2 \propto P_{ICRF}T_e^{3/2}/n_e$, where τ_{SD} is the fast ion slowing down time on electrons. This is because this scaling is strictly valid in the high energy limit with mainly collisional electron heating. However, in the present experimental conditions, according PION, the fast ions are not so energetic and consequently heat predominantly bulk ions in collisions as shown in Fig. 8b. In fact, only in discharges 87869

and 87876 with highest fast ion energy contents of about 150 kJ does the collisional electron heating reach about 40% of the total ICRF power.

Experimental information on the fast proton populations in these discharges is provided by a high-energy neutral particle analyser (NPA) which views that plasma vertically along a line of sight close to the plasma center. As shown in Fig. 9 the measured NPA fluxes increase with W_{fast} as expected.

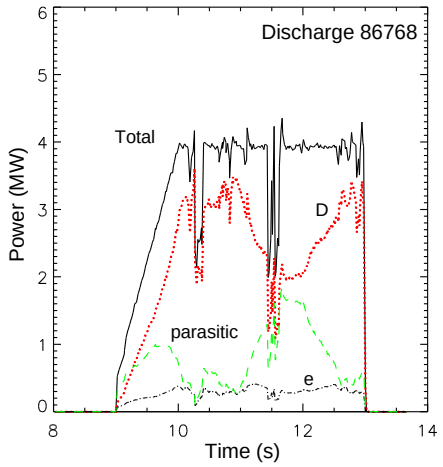

Figure 5 Total ICRF power (black), D damping (red), parasitic edge damping (green) and direct electron damping (dashed black curve) as given by PION for discharge 86768.

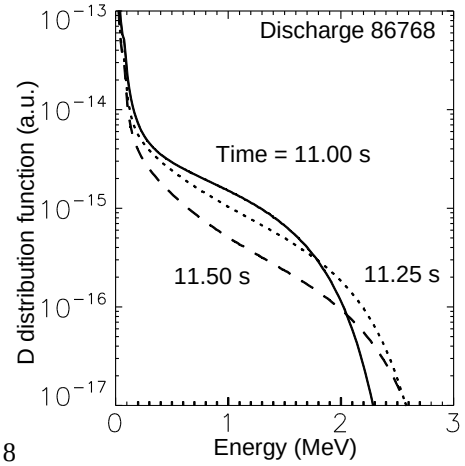

Figure 6 Deuterium distribution function f(v, μ= 0) as given by PION for discharge 86768 with 4 MW of ICRF power tuned to $\omega \approx 3\omega_{cD}$ at t = 11.00 s, 11.25 s and 11.50 s.

(a)

(b)

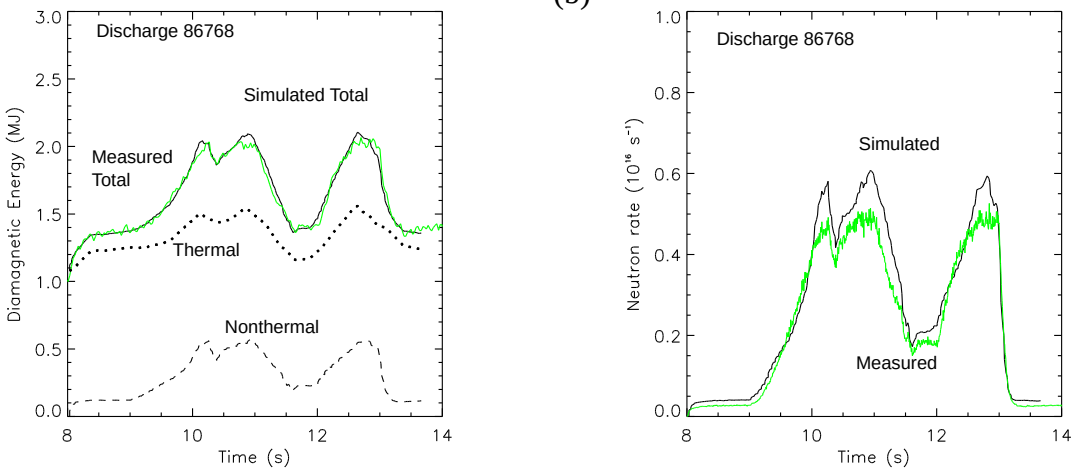

Figure 7 (a) Measured (green) and simulated (solid black) W_{DIA} together with the measured thermal (dotted) and simulated nonthermal (dashed) contributions and (b) measured (green) and simulated (black) R_{NT} for discharge 86768.

6. Conclusions

A number of recent experiments carried out on the JET tokamak using different second and higher harmonic ICRF heating schemes have been successfully simulated with the ICRF code PION. Good agreement between measured and calculated ICRF-related quantities has been obtained including the plasma energy content, fusion yield and the ICRF-driven fast-ion distribution functions.

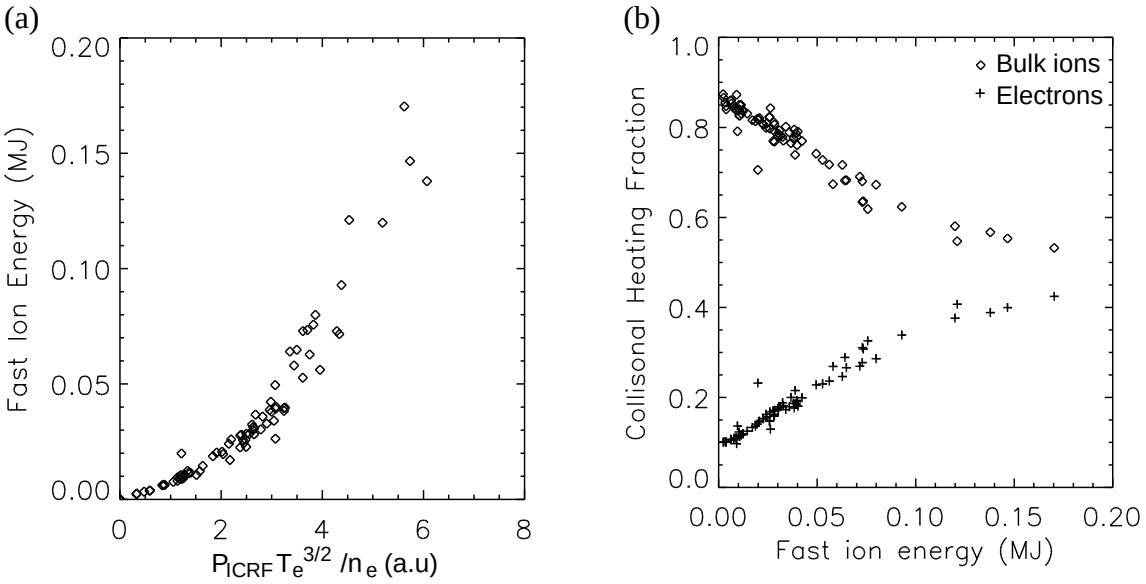

Figure 8 (a) Simulated fast ion energy content W_{fast} as a function of $P_{ICRF}T_e^{3/2}/n_e$ and (b) collisional ion and electron heating fraction as a function of W_{fast} for a series of JET hydrogen discharges with $n_e > 2.5\text{x}10^{19}/\text{m}^3$ and ICRF heating at $\omega \approx 2\omega_{cH}$.

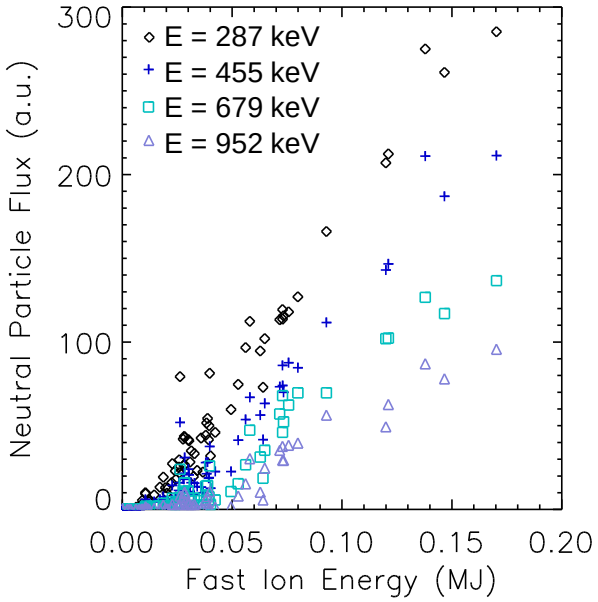

Figure 9 Measured neutral particle hydrogen fluxes at E = 287 keV, 455 keV, 679 keV and 952 keV as a function of simulated fast ion energy content W_{fast} for discharges in Fig. 8.

Among the three ICRF schemes we have studied, third harmonic heating of deuterium has the weakest single pass damping in the absence of an ICRF-driven fast ion tail. For this scenario our results suggest that parasitic edge damping plays an important role, in line with our earlier findings [11]. Furthermore, an improved model for the pitch-angle-averaged ICRF diffusion coefficient has been developed and implemented in the PION code to account for the fall-off of the fast ion population at the location of suppressed wave particle interaction due to finite Larmor radius effects. Overall, our results show that the theoretical picture of high-harmonic heating on which PION is based, is generally correct. This gives confidence in simulations of other experiments in JET and in modelling ICRF heating schemes for ITER and future reactor plasmas.

Acknowledgements This work has been carried out within the framework of the EUROfusion Consortium and has received funding from the Euratom research and training programme 2014-2018 under grant agreement No 633053. The views and opinions expressed herein do not necessarily reflect those of the European Commission.

References

[1] G.F. Matthews et al. Physica Scripta T145 (2011) 014001.
[2] L.-G. Eriksson, T. Hellsten and U. Willén, Nuclear Fusion 33 (1993) 1037.
[3] S. Sharapov et al., "Fast Ion D-D and D-^{3}He Fusion on JET", this conference.
[4] E. Lerche et al., Radio Frequency Power in Plasmas 2015. AIP Conf. Proceedings
[5] M. Gatu Johnson et al., Nucl. Instrum. Methods A, 591 (2008) 417.
[6] M.J. Mantsinen et al., Plasma Physics and Controlled Fusion 41 (1999) 843.
[7] M.J. Mantsinen et al., Nucl. Fusion 39 (1999) 459.
[8] A. Salmi et al., Plasma Phys. Control. Fusion 48 (2006) 717.
[9] M.J. Mantsinen et al., EPS Conference Abstracts 39E, 42nd EPS Conference on Plasma Physics, 2015, Lisboa, Portugal, P2.171.
[10] T. Hellsten et al., Radio Frequency Power in Plasmas 2015, AIP Conf. Proceedings.
[11] L.-G. Eriksson et al., Nuclear Fusion 38 (1998) 265.
[12] M. Schneider et al., "Modelling the synergy between NBI and ICRF waves in JET fusion product studies experiments", this conference.
[13] M. Nocente et al., "Diagnosing MeV range deuterons with neutron and gamma ray spectroscopy at JET", this conference.
[14] D. Anderson et al., Plasma Phys. Control. Fusion 29 (1987) 891.
[15] T.H. Stix, Nuclear Fusion 15 (1975) 737.

Appendix

We introduce a simple model for the pitch-angle-dependent ICRF driven distribution function

$$f(v,\mu) = F(v)\frac{e^{-\left(\frac{\mu}{\Delta\mu(v)}\right)^2}}{\sqrt{\pi}\,\Delta\mu(v)\ \mathrm{erf}\left(\frac{1}{\Delta\mu(v)}\right)} \quad ,$$

where $F(v)$ is the pitch-angle-averaged distribution function and the pitch-angle-dependence of the distribution is characterized by an exponential with a width $\Delta\mu(v)$. We calculate the width $\Delta\mu(v)$ from the effective pitch-angle

$$\mu_{eff}^2(v) = \int_{-1}^{1}\mu^2 f(v,\mu)d\mu \Big/ \int_{-1}^{1} f(v,\mu)d\mu = \frac{[\Delta\mu(v)]^2}{2} - \frac{\Delta\mu(v)}{\sqrt{\pi}}\frac{e^{-\left(\frac{1}{\Delta\mu(v)}\right)^2}}{\mathrm{erf}\left(\frac{1}{\Delta\mu(v)}\right)},$$

using the approximation [14]

$$\mu_{eff}^2(v) = \frac{1}{3}\frac{1+\left(\frac{v}{v_*}\right)^2}{1+\left(\frac{v}{v_*}\right)^2+\left(\frac{v}{v_*}\right)^4} \quad ,$$

where $v_* = 0.5v_\gamma$ and v_γ is the characteristic velocity associated with pitch angle scattering [15]. Finally, we use this distribution to calculate the pitch-angle-average of $D_{RF}(v,\mu)$ as

$$\int_{-1}^{1} D_{RF}(v,\mu)f(v,\mu)d\mu \Big/ \int_{-1}^{1} f(v,\mu)d\mu = \int_{-1}^{1} D_{RF}(v,\mu)\frac{e^{-\left(\frac{\mu}{\Delta\mu(v)}\right)^2}}{\sqrt{\pi}\ \Delta\mu(v)\ \mathrm{erf}\left(\frac{1}{\Delta\mu(v)}\right)}d\mu.$$